Optical and Quantum Electronics (2024) 56:483
https://doi.org/10.1007/s11082-023-06082-z

A new SOI sensor design for detecting cancer using hybrid waveguide with higher sensitivity than both strip and slot waveguides

Sherine Shawky[1] · Ahmed H. Abd El-Malek[1] · Ahmed Allam[1] · Hossam M. H. Shalaby[2]

Received: 14 August 2023 / Accepted: 10 December 2023 / Published online: 27 January 2024

Abstract
A new highly accurate optical biomedical sensor is proposed for cancer detection characterized by high sensitivity, small footprint, low cost, and low limit of detection. The sensor is based on double-ring resonators made of silicon on insulator. The type of the waveguide is critical in determining the sensor performance. To compromise the advantages and disadvantages of strip and slot waveguides, a mixed design of both has been introduced in literature at the expense of increased footprint compared to traditional sensors. Indeed, almost 27-fold footprint increase is required to improve the sensitivity by only one third of that of slot waveguide's sensitivity. In this paper, we introduce a new design that keeps the same footprint of traditional sensors, while achieving high sensitivity. This sensitivity depends on the resonance wavelength shift due to different refractive indices of the biosample. It has the value 109.8 nm/RIU compared to 55.57 nm/RIU and 129.621 nm/RIU for strip and slot waveguides, respectively. The hybrid waveguide quality factor is 537.7 while the quality factors of the strip and the slot waveguides are 627.99 and 380.76, respectively. In addition, the new design achieves the minimum limit of detection (0.0255) when compared to that of traditional designs. Furthermore, a new method of detection is proposed with the same design, providing a higher sensitivity over both traditional waveguide types with a value of 15.3, compared to 13.2 and 11.5 for strip and slot waveguides, respectively. In this method, the sensitivity relies on various values of output transmitted light at the same wavelength due to altering the biocell refractive index. The biosensor output equation is developed. In addition, the relationship between the supermodes and the sensitivity is determined at variance conditions. It is found that there is an inverse relation between them.

Keywords Optical biosensor · Double optical ring resonator · Silicon on insulator · Hybrid waveguide

Extended author information available on the last page of the article

1 Introduction

The research of early detection of cancer diseases is on rise every day and becoming an essential life tradition. This is because the failure of finding a complete treatment for it, leading to losing a human life (Panda and Pukhrambam 2020; Eskandarinezhad et al. 2022). In fact, it is the reason of the death of one person from six persons with the ability of increasing this number (Hussain et al. 2021). According to the World Health Organization (WHO), the new cancer cases are around 20 million with almost half of them died until 2020 (Ferlay et al. 2021). It is also expecting a rise in the number of new cases to be approximately 29 million in 2040 (Sung et al. 2021). On the other hand, early detection of the disease reduces the pain that the cancer patient would suffer due to late treatment such as chemical, radiational, or surgical treatment (Azab et al. 2023). Cancer is considered a genetic disease due to an error in cell division causing deoxyribonucleic acid (DNA) damage by harmful substances (Kumar et al. 2019). It is a continuous reproduction of aimless and unwanted cells. Unfortunately, it can appear and grow abnormally in any part of the human body adding to spreading to the neighboring organs in the human body. This expanse of cancer is called metastasis and it makes it more threatening and deadly. This uncontrollable growth rate of these cancerous cells cause tumors (Azab et al. 2023; C et al. 2022; Ragavendran et al. 2023).

Imaging, lab tests, and tissue biopsy are the conventional methodologies to diagnose cancer. computerized tomography (CT), Magnetic resonance imaging (MRI), and X-ray (Azab et al. 2023) are examples for imaging modalities and are used to get a detailed images of the infected organ. If the image indicates that the organ has tumors, then this patient is diagnosed as a cancer patient. Lab test is a quantitation of biomarkers in physiological fluid. The patient's urine or blood are analyzed and if a biomarker related to cancer is obtained, an indication for the presence of cancer is given. Another method to detect cancer is to get just a tissue from the patient and by using a microscope, a decision is taken whether the tissue is cancerous or not (Vaidyanathan et al. 2018; Hussain et al. 2021; Panda and Pukhrambam 2020). Unfortunately, all these methodologies are taken place in late stages after already the cancer spread through the organ or the body. It is very hard to detect the cancer disease in early stage. The reason for that is the need for a highly qualified professional pathologist (Vaidyanathan et al. 2018). In addition, millions of cells are needed for the detection approach which is missing in the early stage of the disease (Sharifian Jazi et al. 2022; Hsieh et al. 2016) and the concentration of the biomarker is not enough for their diagnosing techniques.

To overcome these drawbacks, a new technology has to be developed in order to replace these ones (C et al. 2022). Biosensors are a promising solution for that. They are defined as an analytical device to detect certain biological interaction (Hussain et al. 2021). They introduce better characterizations including low cost, high performance, reproducibility, high reliability, high accuracy, and low response time (Hussain et al. 2021). In addition, they do not need a highly qualified person to use them like the other methods where any one can use them easily (Naresh and Lee 2021).

Biosensors can be classified into two types which are biorecognition based and transduction based (Naresh and Lee 2021). The biorecognition-based sensors depend on a specific interaction between a bioreceptor and a test sample. This interaction may be catalytic or affinity. The transduction-based sensors depend on a change in certain property of the sample being detected. Thermal, chemical, mechanical, electrochemical, piezoelectrical, and optical are examples for this property (Guck et al. 2005; Suresh 2007; Park et al. 2005).

The sensing of any disease which depends on the photonic concepts provides a precisely approach through analyzing the human's urine or blood (Uddin et al. 2020). Biosensors based on optical properties such as emission, absorption, fluorescence, refractometry, and polarimetry are called optical biosensors (Lechuga 2005). Optical sensors have the ability to detect multiple analytes via multiplexed systems (Nordin 2016). They have many other advantages such as low cost, immunity to other electromagnetic fields and real time detection (Guo et al. 2011). The protein presence in the cancerous cell is bigger than that found in the normal cell due to the high rate of its growth. So, the interaction between the light and the cell will differ if the cell is malignant. Accordingly, we can distinguish whether the cell is cancerous or not through its refractive index (Azab et al. 2023). In addition, different types of cancer disease can be determined.

1.1 Literature review

Silicon on insulator technology is the best choice for biosensing applications especially when using optical microring resonators (Ghasemi et al. 2016). In (Ghasemi et al. 2016), the sensitivity reached 49 nm/RIU and in Yan et al. (2016), the sensitivity is 44.6 nm/RIU. Some developed ideas for micro ring resonators have been investigated to enhance the sensitivity like subwavelength grating (Huang et al. 2017). The sensitivity obtained in Huang et al. (2017), is 429.7 nm/RIU. But this method is very complex and hard to be fabricated. In Zhao et al. (2018), the sensitivity reached 297.13 nm/RIU, but this design has a large footprint. In optical sensors, the key idea is to find a design that allows light to leak into the surrounding material, like vertical nanowire sensors or suspended waveguides (Mohamed et al. 2019). That is, the more leaking light, the better performance for the optical sensor (Elsayed et al. 2020). The sensitivity reaches 100 nm/RIU in Mohamed et al. (2019) and it has a large footprint. In Elsayed et al. (2020), the sensitivity reached 330 nm/RIU but they used the multimode interference structure.In other words, the sensing of a disease relies on the remarkable difference between the refractive index of the normal and the infected cells utilizing the evanescent nature of the light. And in De Vos et al. (2007) is 70 nm/RIU.

Accordingly, slot waveguides can be good choices for biosening as they provide high sensitivity. However, they suffer from high optical losses. On the other hand, strip waveguides have low optical losses, but they do not achieve better sensitivity than slot waveguides. To solve this dilemma, a hybrid design between slot and strip waveguides have been introduced in Steglich et al. (2017). However, this design increases the traditional footprint by extra 2620 µm, which means increasing the area of the conventional sensor with 27 fold than its value. In addition, it has only achieved a sensitivity that represents 36% of the slot sensitivity and 152% of the strip waveguide. The sensitivity in this design is 106.29 nm/RIU.

1.2 Aim of paper

In this paper, we propose a new highly sensitive sensor with a design that keeps the same footprint of the traditional sensors without any rise in its size or cost. The proposed design consists of a double-ring resonator with two bus waveguides. The ring waveguide is a mix between strip and slot waveguides where it has a slot from angle −60° to angle 60° with respect to x-axis. This allows more light to interact with the biosample fluid. In order to keep the advantages of the strip waveguide, the bus waveguides are not of the slot type.

The new design improves the sensitivity of the hybrid waveguide to 85% and 198% of that of the slot and the strip waveguides respectively.

This sensitivity improvement is based on a shift in the resonance wavelength. Moreover, we introduce another method of sensing process with another concept of sensitivity that is based on the difference in transmission of light intensities. The later sensitivity is found to be higher than both that of slot and strip waveguides. In addition, the new design achieves the minimum limit of detection (of 0.0255 μm) when compared to that of both strip and slot waveguides. The relation between the total supermodes of the new design and the sensitivity, based on resonance wavelength shift, is discussed as well with different conditions. It is found that there is an inverse correlation between the number of supermodes and the sensitivity.

There is some work that reaches sensitivity of 311.97 nm (Long et al. 2022), and 494 nm. Haibin et al. (2022). But, these publications used plasmonics which is too costly and need some complex operations for fabrication due to the need of specialized materials and fabrication techniques (Guo et al. 2015). On the other hand, SOI is cost-effective, especially for large-scale production due to its compatible with existing semiconductor fabrication process (Kianisarkaleh et al. 2017). By comparing our biosensor with recent paper with the same technique SOI, we reached a sensitivity of 109.8 nm. with a footprint of only 135.127 μm^2. while in Steglich et al. (2017), the sensitivity is 106.29 nm with the footprint is 2720 μm^2. Also, in CHEN et al. (2022), the sensitivity is 104 nm. Besides, our biosensor introduces a higher sensitivity than plasmonics as in Silva et al. (2022), the achieved sensitivity is only 33 nm.

1.3 Paper organization

The remaining of this paper is organized as follows. The mathematical model of the biosensor is given in Sect. 3. Section 4 is devoted for the evaluation of system performance and discussion of results. Finally, the conclusion is presented in Sect. 5.

2 Proposed biosensor structure

Figure 1 illustrates the different structures of the biosensor based on the type of waveguide. The red arrow presented in Fig. 1 shows the input field direction, and the green one indicates the output field. It is clear that the footprint of the proposed biosensor is kept constant

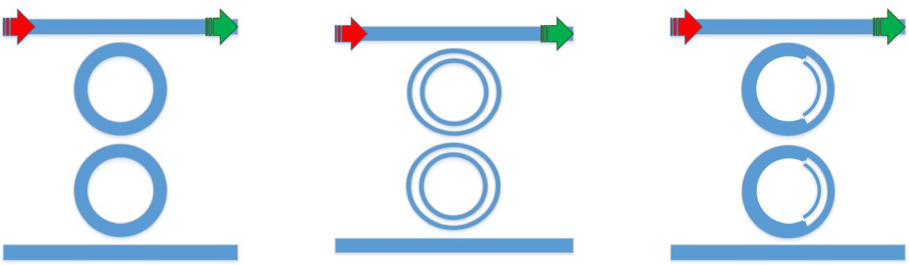

Fig. 1 The structure of the biosensor according to waveguide type: **a** Strip. **b** Slot. **c**Hybrid

as the traditional waveguide types. The design of all types consists of SOI with Si height of 0.22 µm inside the buried oxide layer (BOX), and 0.22 µm height above it. While the BOX height is 4 µm. The other parameters such as ring resonator (RR) radius, waveguide width, and the gap between waveguides are chosen as in 4.1

3 Mathematical model

The general equation of the output normalized transmission T (unitless) for all types of waveguides is the same and can be found from the following equation:

$$T = \frac{\begin{array}{c} v_1^2 + v_1^2 v_2^2 v_3^2 u_2^2 - 2v_1^2 v_2 v_3 u_2 \cos\theta_2 + v_2^2 u_1^2 + v_3^2 u_1^2 u_2^2 - 2v_2 v_3 u_1^2 u_2 \cos\theta_2 - 2v_1 v_2 u_1 \cos\theta_1 \\ +2v_1 v_3 u_1 u_2 \cos\theta_1 \cos\theta_2 + 2v_1 v_2^2 v_3 u_1 u_2 \cos\theta_1 \cos\theta_2 - 2v_1 v_2 v_3^2 u_1 u_2^2 \cos\theta_1 \end{array}}{\begin{array}{c} 1 + v_2^2 v_3^2 u_2^2 - 2v_2 v_3 u_2 \cos\theta_2 + v_1^2 v_3^2 u_1^2 u_2^2 - 2v_1^2 v_2 v_3 u_1^2 u_2 \cos\theta_2 - 2v_1 v_2 u_1 \cos\theta_1 \\ +v_1^2 v_2^2 u_1^2 + 2v_1 v_3 u_1 u_2 \cos\theta_1 \cos\theta_2 - 2v_1 v_2 v_3^2 u_1 u_2^2 \cos\theta_1 + 2v_1 v_2^2 v_3 u_1 u_2 \cos\theta_1 \cos\theta_2 \end{array}}. \tag{1}$$

This equation is obtained from the following transfer function (Kedia and Gupta 2015):

$$H = \frac{v_1 - v_1 v_2 v_3 e^{-j\theta_2} u_2 - v_2 e^{-j\theta_1} u_1 + v_3 e^{-j\theta_1} u_1 e^{-j\theta_2} u_2}{1 - v_2 v_3 e^{-j\theta_2} u_2 - v_1 v_2 e^{-j\theta_1} u_1 + v_1 v_3 e^{-j\theta_1} u_1 e^{-j\theta_2} u_2} \tag{2}$$

after substituting in $T = |H|^2$. v_i (unitless) represents the coupling portion of the propagating field where $v_i = \cos(\kappa_i Lc_i)$. κ (m^{-1}) is the coupling coefficient, Lc_i (m) is the coupler's length and $i \in \{1, 2, 3\}$ represents the region of coupling as follows: $i = 1$: coupling between the upper bus waveguide and the upper ring. $i = 2$: coupling between the two rings. $i = 3$: coupling between the lower bus waveguide and the lower ring. u_j (unitless) and θ_j (rad) represent the attenuation loss and the phase shift due to passing in the rings where $u_j = e^{-\frac{\alpha_j L_j}{2}}$ and $\theta_j = \beta_j L_j$. α_j (m^{-1}) is the attenuation coefficient and β_j (rad/m) is the propagation constant. L_j (m) is the path traveled by the field where $L_j = 2\pi r_j$ as r_j (m) is the radius of the ring and $j \in \{1, 2\}$ represents the upper and lower rings, respectively.

The sensitivity S (nm/RIU) of the proposed design can be calculated from Steglich et al. (2017):

$$S = S_{wg} S_{rr} = \frac{\Delta n_{eff}}{\Delta n_{clad}} \frac{\Delta\lambda}{\Delta n_{eff}} = \frac{\Delta\lambda}{\Delta n_{clad}}, \tag{3}$$

where S_{wg} is the waveguide sensitivity, S_{rr} is the sensitivity of ring resonator, Δn_{eff} and Δn_{clad} are the changes in the effective and cladding refractive indices, respectively, and $\Delta\lambda$ is the resonance wavelength shift. This change in resonance wavelength occurs due to the presence of a cancerous cell in contact with the sensing area of the biosensor, leading to a change in the effective refractive index. Each type of cancer disease has a certain refractive index as listed in Table. 1.

To estimate the performance of the proposed design, the optical quality factor Q (unitless) is determined from Steglich et al. (2017):

$$Q = \frac{\lambda_{res}}{FWHM}, \tag{4}$$

Table 1 Refractive index (RI) of biosamples (Ali et al. 2020)

Name of biocell	Disease	RI	Name of biocell	Disease	RI
Normal		1.350	PC-12	Brain cancer	1.395
Jurkat	Leukemia	1.390	MDA-MB-231	Breast cancer	1.399
HeLa	Cervical Cancer	1.392	MCF-7	Breast cancer	1.401

where λ_{res} is the resonance wavelength and FWHM is the full width half maximum. In addition, the intrinsic limit of detection *iLOD* (unitless) is found from Steglich et al. (2017):

$$iLOD = \frac{\text{FWHM}}{S}. \tag{5}$$

4 Results and discussion

4.1 Changing waveguide parameters

Here, the effect of changing some parameters in waveguide design is discussed. These parameters include waveguide width, gap between waveguides, and ring resonator radius. In all waveguide types, we started changing the waveguide width followed by varying the gap between waveguides and finally altering the ring resonator radius. In every stage, we selected the optimized value which achieved the maximum sensitivity side by side with a good readable output signal. The sensitivity was calculated using six refractive indices which represent the normal cell and the cancerous cells of different types. The output signal for each value of the parameter in a certain region was drawn using the normal cell refractive index to choose the readable one with the highest sensitivity. We use finite-difference time-domain to perform this study. Lumerical FDTD is utilized here and the FDTD parameters' values are listed in Table 2. All boundaries are perfect matched layer (PML). The monitor frequency points are 500. The fundamental mode is the propagating mode.

Table 2 FDTD parameters

Parameter	Value
Dimension	3D
Simulation time	4000
Simulation temperature (K)	300
Background material	air
Mesh accuracy	1
x (μm)	0
x span (μm)	8.52
y (μm)	0
y span (μm)	15.86
z (μm)	−0.5
z span (μm)	4

4.1.1 Strip waveguide

Waveguide width

The waveguide width w_{strip} is changed from 0.1 μm to 0.4 μm with step 0.01 μm. Although, we know that 0.1 μm is very small width that light cannot propagate through, but, we started from this value to pick the first suitable value that allows the light propagation with a high sensitivity. The width for all waveguides (upper and lower buses, and two ring resonators) present in the strip type are changed equally. The output normalized transmission spectrum is shown in Fig. 2a for certain values of w_{strip}. At $w_{\text{strip}} = 0.34\,\mu\text{m}$, the output spectrum has a very good shape and can be detected easily but at this value, the sensitivity is low. On the other side, when $w_{\text{strip}} = 0.14\,\mu\text{m}$, the sensitivity is high while the output spectrum is not readable. Accordingly, both values are rejected. The chosen value is 0.26 μm because it has an accepted shape for the output spectrum with a good sensitivity compared with the other values. The sensitivity is found in the range of changing width from 0.24 μm to 0.4 μm with step 0.01 μm because the output is clear in this range. The sensitivity is shown in Fig. 2b and it is found that the sensitivity is decreasing when increasing the width of waveguide.

This inverse relation is compatible with the optical biosensor concept as the biosensor sensitivity depends on the amount of light outside the waveguide. So, the wider the waveguide width corresponds to a lower sensitivity and vice versa. The small variation up and down is an accepted error. The values from 0.2 to 0.27 μm vary more far from the fitted curve than the other values due to the tail peaks of the field (Kedia and Gupta 2017). When the width is small these peaks are outside the waveguide causing presence of more light interacting with the bio-sample. These peaks' positions are around 0.27 μm and their exact positions vary according to the cladding's refractive index (Kedia and Gupta 2017). The values which are larger than that range allows the presence of these peaks inside the waveguide, therefore, less light presents in the contact area with the bio-sample.

Gap between Waveguides

The gap between each two waveguides $L_{\text{gap-strip}}$ is changed equally from $L_{\text{gap-strip}} = 10\,nm$ to $L_{\text{gap-strip}} = 260\,nm$ with step $L_{\text{gap-strip}} = 5\,nm$. Figure 3a illustrates the normalized transmission at $L_{\text{gap-strip}} = 10\,nm$, $L_{\text{gap-strip}} = 260\,nm$, and $L_{\text{gap-strip}} = 100\,nm$.

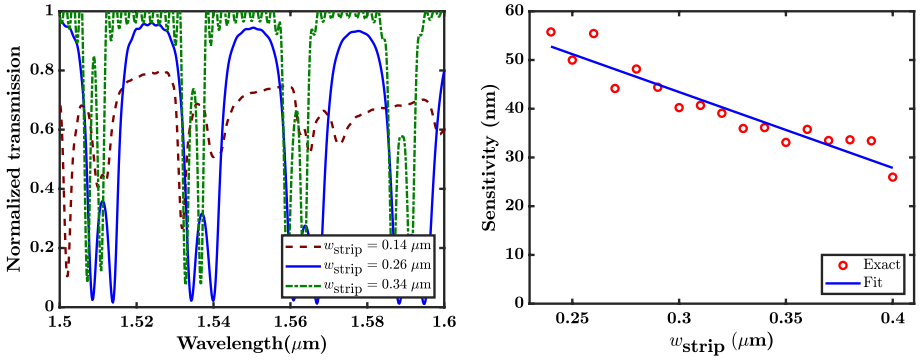

Fig. 2 **a** The output normalized transmission spectrum at different values of strip waveguide width (w_{strip}). **b**The sensitivity when changing (w_{strip}

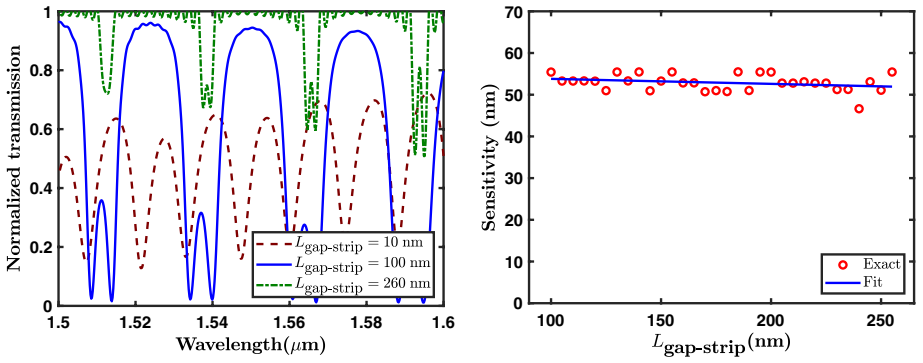

(a) (b)

Fig. 3 **a** The output normalized transmission spectrum at certain values of the gap between strip waveguide ($L_{\text{gap-strip}}$).**b** The sensitivity when changing $L_{\text{gap-strip}}$

At the first two values, the shape of the normalized transmission is not accepted, while the last value has a good readable shape. Figure 3b demonstrates the sensitivity when changing the $L_{\text{gap-strip}}$ in the range of 100 nm and 255 nm. It is found that there is no change in the sensitivity when changing $L_{\text{gap-strip}}$.

Ring resonator radius The radius of both ring resonators r_{strip} is changed equally from 0.4 μm to 5 μm with step of 0.1 μm. The output transmission spectrum when $r_{\text{strip}} = 0.8, 2.5,$ and 4 μm is demonstrated in Fig. 4a. It is clear that the sensitivity is constant over the range between 0.8 μm and 3 μm. We select $r_{\text{strip}} = 2.5$ μm because it has a good sensitivity with an easily detectable output curve.

4.1.2 Slot waveguide

Waveguide width

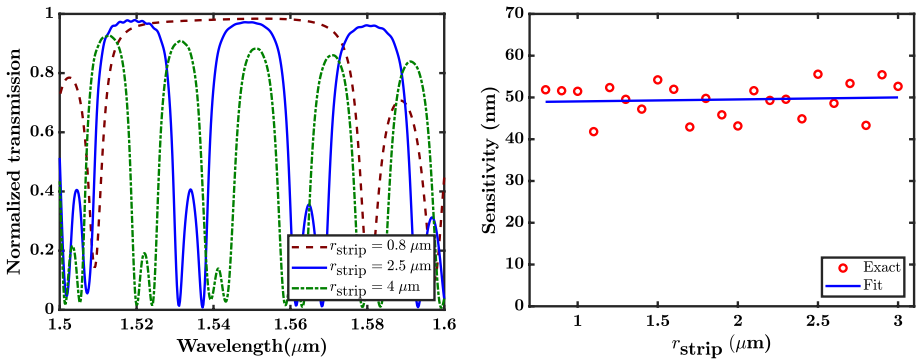

(a) (b)

Fig. 4 **a** The output normalized transmission spectrum at some points of RR radius of the strip waveguide (r_{strip}). **b**The sensitivity when altering r_{strip}

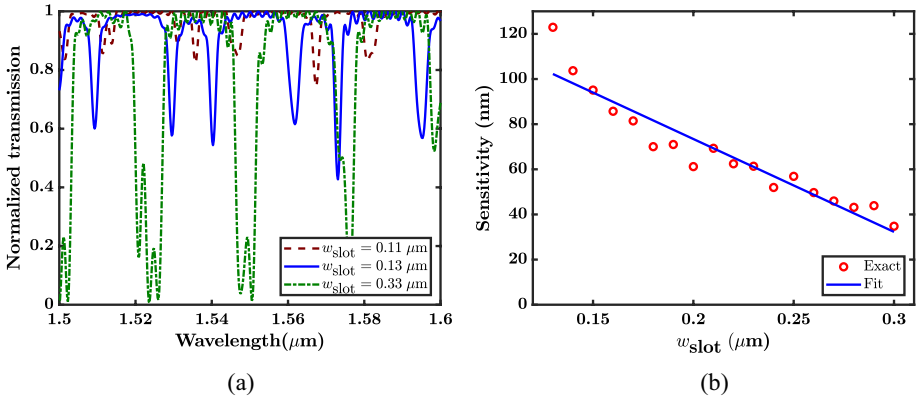

Fig. 5 **a** The output normalized transmission spectrum at different values of slot waveguide width (w_{slot}). **b**The sensitivity when changing w_{slot}

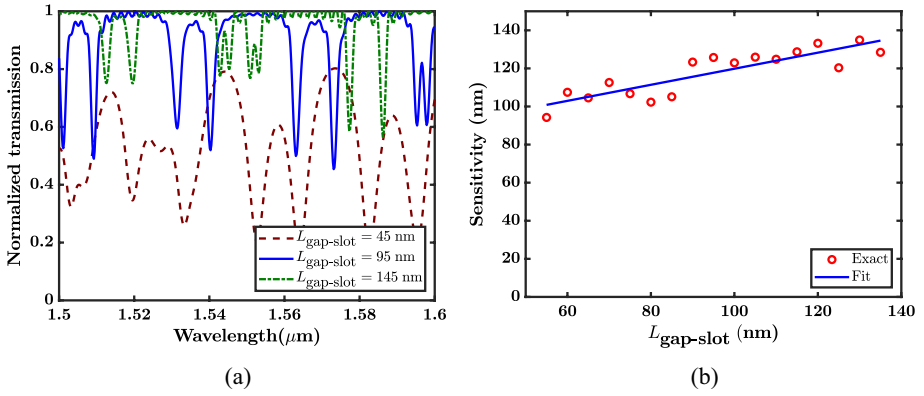

Fig. 6 **a** Output normalized transmission spectrum at certain values of the gap between the slot waveguide ($L_{gap-slot}$). **b** Sensitivity when changing $L_{gap-slot}$

The width of the bus waveguide remains constant with value 0.26 μm which represents the best value found in the strip calculation in Sect. 4.1.1. Here, the width of the slot waveguides w_{slot} present in the two ring resonators is altered from 0.05 nm to 0.4 μm with a step of 0.01 μm. Figure 5a shows the output normalized transmission spectrum versus w_{slot} in order to find the effect of changing w_{slot} on it. Similarly as in Sect. 4.1.1, we reject $w_{slot} = 0.11\,\mu m$ because its spectrum is not clear to be detected although it has a high sensitivity. Also, $w_{slot} = 0.33\,\mu m$ is rejected due to its low sensitivity. An in-between value $w_{slot} = 0.13\,\mu m$ is selected. Figure 5b shows the sensitivity over the range from $w_{slot} = 0.13\,\mu m$ to $w_{slot} = 0.3\,\mu m$, where it has a similar behavior to that of the strip waveguide.

Gap between waveguides

The gap between the slot ring resonator waveguides is altered equally with all the other gaps between waveguides in the same range as in strip waveguide. Some selected output normalized transmission spectrum are displayed in Fig. 6a, where $L_{gap-slot} = 45\,nm$ and

$L_{\text{gap-slot}} = 145\,nm$ are the forbidden numbers, while $L_{\text{gap-slot}} = 100\,nm$ is the chosen one. The sensitivity is calculated when $L_{\text{gap-slot}} = 55\,nm$ to $L_{\text{gap-slot}} = 135\,nm$ as viewed on Fig. 6b. There is a slight raise in the sensitivity while increasing the $L_{\text{gap-slot}}$. We choose 100 *nm* to couple a good amount of power as it has the highest sensitivity as shown in 6b.

Ring resonator radius

In this part, the radius parameter is changed in the same way as that in strip waveguide. Figure 7a illustrates some output spectra at 0.7 µm, 2.5 µm, and 4.1 µm. The behavior of the sensitivity is also the same as that in strip waveguide but over a different range from 1.4 µm to 3 µm as displayed in Fig. 7b. The value 2.5 µm is chosen as in strip waveguide.

4.1.3 Hybrid waveguide

Waveguide width

Here we follow same methodology used for both stip and slot waveguides, but now for the hybrid waveguide. Both $w_{\text{hybrid}} = 0.08\,\mu\text{m}$ and $w_{\text{hybrid}} = 0.18\,\mu\text{m}$ are the rejected values of w_{hybrid} while $w_{\text{hybrid}} = 0.1\,\mu\text{m}$ represents the accepted one as clear in Fig. 8a. The sensitivity in this case is shown in Fig. 8b having an inverse relation with w_{hybrid}.

Gap between waveguides

Again but for hybrid waveguide, Fig. 9a lays out the output spectrum for selected points at which $L_{\text{gap-hybrid}} = 30, 100$, and $200\,nm$. The taken point is 100 nm for the same reason as in the case of slot waveguide. Figure 9b demonstrates the sensitivity in the range 70 nm to 155 nm.

Figures 3b, 6b, and 9b are compared which represent the relation between the sensitivity and the gap between waveguides for strip, slot, and hybrid waveguides, respectively. It is found that it is almost constant for strip but there is a significant increase for slot and a small rise in the case of hybrid. Actually, it is increasing in all cases but it appears as if it is stable in the case of strip because the increase is not large enough and can be neglected. This is because of the principle of the optical biosensors where the larger the area of contact with the blood, the greater value of the sensitivity. In the case of strip waveguide, the contact area is almost the same, increasing the gaps between the waveguides is not big enough to increase the contact area by a notable value, while in case of the slot waveguide it is large because the gaps not

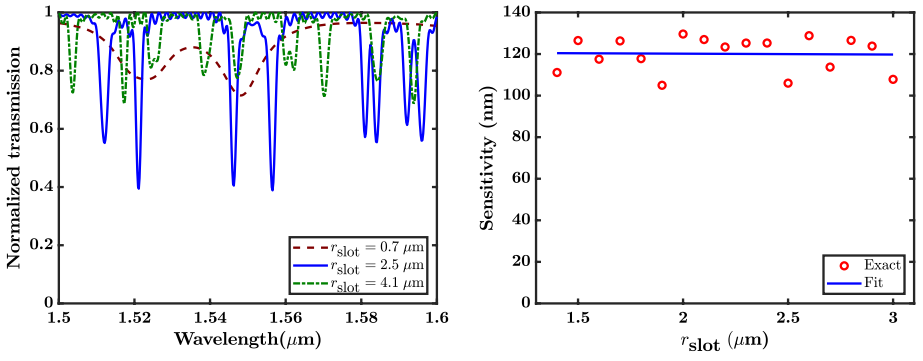

Fig. 7 **a** Output normalized transmission spectrum at some points of the RR radius of the slot waveguide (r_{slot}). **b** Sensitivity when altering r_{slot}

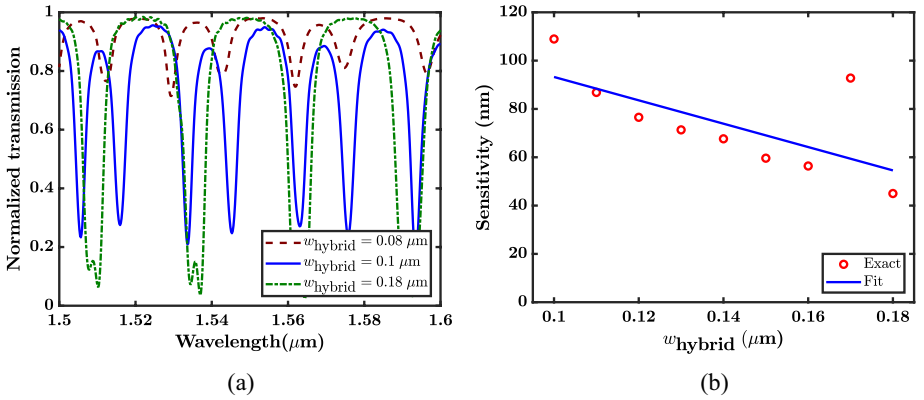

Fig. 8 **a** Output normalized transmission spectrum at different values of the hybrid waveguide width (w_{hybrid}). **b** Sensitivity when changing w_{hybrid}

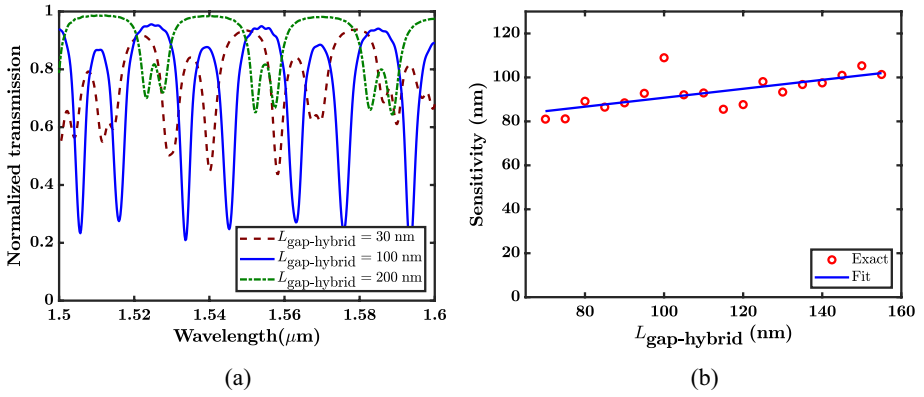

Fig. 9 **a** Output normalized transmission spectrum at certain values of the gap between the hybrid waveguide ($L_{gap-hybrid}$). **b** Sensitivity when changing $L_{gap-hybrid}$

only present between the waveguides but they also present inside each waveguide. So, this makes the contact area larger with a considerable amount. By looking to the case of hybrid waveguide, it is intermediate case between strip and slot and it is clear from Fig. 9b that the rise is not as large as slot and not as very small as strip.

Ring resonator radius

The same is done here as in strip and slot waveguides. Three values of r are shown in Fig. 10a which are 1.1 μm, 2.5 μm, and 4.1 μm. The sensitivity is almost the same at all values of r_{hybrid} from 1.7 μm, to 3.7 μm, as shown in Fig. 10b. Like in strip and slot waveguides, 2.5 μm is selected for the optimized value.

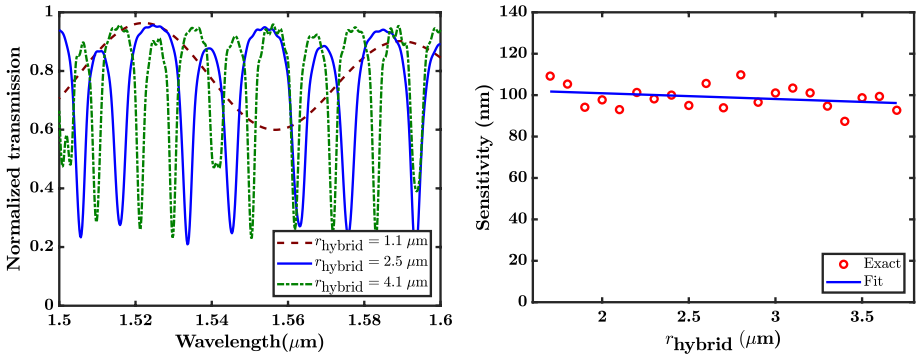

(a) (b)

Fig. 10 **a** Output normalized transmission spectrum at some points of the RR radius of the hybrid waveguide (r_{hybrid}). **b** Sensitivity when altering r_{hybrid}

4.2 Output transmission spectrum

In this section, the output spectrum of the normalized transmission is calculated using the optimized parameters found in Sect. 4.1 for each type of waveguides. Figures 11, 12, and 13 shows the output spectrum using three kinds of waveguides for the normal cell and the infected cells with various cancer types. Zoom curves are displayed in the same figures in order to show the shift in resonance wavelength for each cancer kind. This shift in resonance wavelength is caused by the change in refractive index due to the presence of cancerous cell.

4.3 Comparison between new design with traditional ones

To find out the enhancement of the sensing operation using the introduced design, some measurements are performed in Table 3.

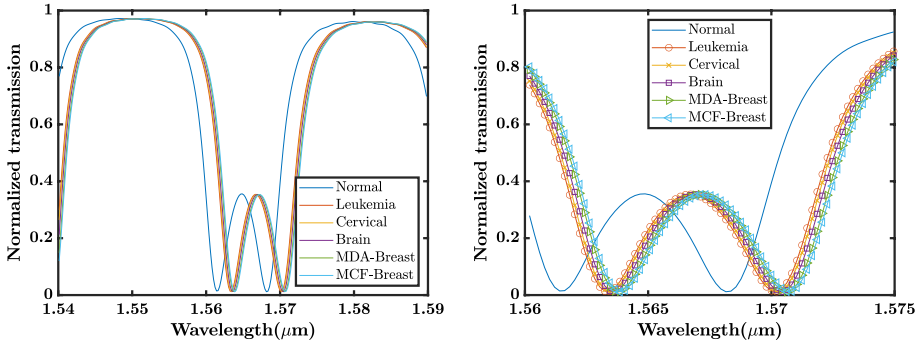

(a) (b)

Fig. 11 **a** The output spectrum of the sensor when using the strip waveguide. **b** zoom in for (a)

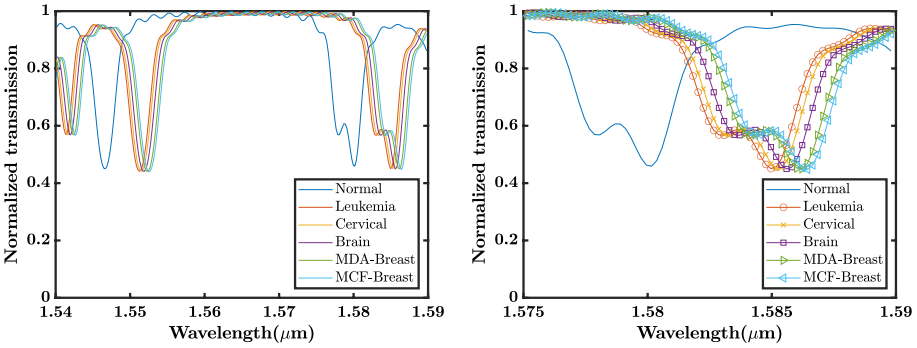

Fig. 12 **a** The output spectrum of the sensor when using the slot waveguide. **b** zoom in for (a)

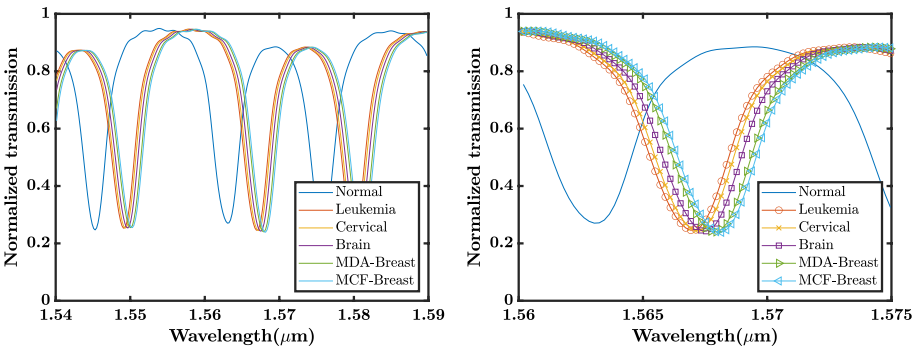

Fig. 13 **a** The output spectrum of the sensor when using the hybrid waveguide. **b** zoom in for (a)

Table 3 Evaluation of some parameters to measure the performance of proposed sensor compared with traditional ones depending on type of waveguide

Performance measure	Strip	Slot	Hybrid	Percentage of achievement
S [nm/RIU]	55.57	129.621	109.8	85 % Slot
Q	627.99	380.76	537.7	86 % Strip
iLOD	0.04318	0.032	0.0255	−20.3 % Strip
FWHM [nm]	2.4	4.15	2.8	-17 % Strip

These parameters are sensitivity S, quality factor Q, intrinsic limit of detection *iLOD* and FWHM. The sensitivity of the strip waveguide is 55.57 nm and that of the slot waveguide is 129.621 nm but the sensitivity of the proposed hybrid design is 109.8 nm. By comparing between various types of waveguides, we find that the hybrid sensitivity is almost double that of strip sensitivity and reaches about 0.85 of slot sensitivity. Besides, the quality factor is 627.99 and 380.76 for the strip and slot waveguides, respectively, while the

Table 4 Another measure for the performance of each sensor using a different definition of sensitivity

	Strip		Slot		Hybrid	
	Max	Min	Max	Min	Max	Min
S	13.225	−13.357	11.477	−11.293	15.2778	−13.732
λ	1.531	1.540	1.593	1.599	1.593	1.599

Table 5 Number of supemodes and corresponding sensitivity in the case of strip waveguide

w_{strip} (μm)	M (modes)	S (nm)
0.4	24	25.97
0.33	21	35.95
0.26	18	55.43

hybrid waveguide has in-between quality factor of 537.7. This represents 86% and 141% of that of strip and slot waveguides, respectively. The introduced hybrid design achieves the minimum for *iLOD* with value of 0.0255 versus 0.04318 and 0.032 for that of strip and slot waveguides, respectively. Finally, the FWHM of the hybrid waveguide is 2.8 nm, too close to that of strip waveguide, which is 2.4 nm, while 4.15 nm is the corresponding value for slot waveguide.

4.4 Transmission power sensitivity

In this section, we define another sensitivity measurement technique, based on the change in normalized transmission power at certain wavelength. Specifically, at a specified value for wavelength, the normalized transmission power is determined for the normal cell and all infected cells. The wavelength is chosen according to the maximum and the minimum sensitivity found in the range of $\lambda = 1.5\,\mu m$ to $\lambda = 1.6\,\mu m$. The sensitivity is determined in all wavelengths in the above range and the results are recorded in Table 4. It demonstrates the prevalence of the new hybrid design over the traditional waveguide designs where it provides the highest sensitivity. Max and Min in Table 4 represent the maximum and the minimum sensitivity, respectively.

4.5 Relation between number of supermodes and sensitivity

In this subsection, the relation between the number of supemodes and sensitivity is found out. The number of supemodes is determined using Lumerical MODE and the sensitivity is evaluated using Matlab. The results are presented in Table 5. It is clear that the number of produced supemodes in the sensor design is inversely proportional with the waveguide width. This is consistent with silicon photonics theories as when the waveguide width shrinks, the excitation of the modes also decreases. Besides, the sensitivity of the whole system rises because the propagating light inside the waveguide is not confined.

By keeping the unslotted waveguides with the same chosen width of 0.26 μm, the number of supemodes produced in both slot and hybrid waveguides are determined as shown in Table 6. It is clear that the numbers of produced supemodes in sensors based on slot and hybrid waveguides are lower than that based on strip waveguide. The senistivities in both cases are also higher than that found in strip design.

Table 6 Number of supemodes and corresponding sensitivity in the case of slot and hybrid waveguides while keeping the bus waveguide constant with value 0.26 µm

Slot			Hybrid		
w_{slot} (µm)	M (modes)	S (nm)	w_{hybrid} (µm)	M (modes)	S (nm)
0.2	20	61.19	0.2	20	44.31
0.16	19	85.72	0.16	19	56.38
0.13	19	122.93	0.13	18	71.34

To study the effect of the number of super-modes on the sensor sensitivity, the widths of the unslotted parts of the waveguides (w) are changed as well as the widths of the slotted ones (w_s), as illustrated in Table 7. Studying carefully this table, it is clear that the sensitivities of slot waveguide are slightly higher when increasing w with w_s. But, in the case of hybrid waveguide, there is almost no change in its sensitivities either keeping w constant or not.

By looking at each row either in Table 6 or 7, it is found that there is an inverse correlation between the number of supermodes and the sensor sensitivity.

4.6 Number of supermodes at different projections

By using the optimum values found in Sect. 4.1, the position of the FDE projection is changed from $x = -5.5$ µm to $x = 5.5$ µm, by step of 0.5 µm. Table 8 illustrates the number of supermodes at each projection. At the edges of the design, we have 6 supermodes (3 TE and 3 TM), which is expected as we have 3 different coupling regions.

4.7 Effect of changing gap on sensitivity

In section 4.1, the sensitivity is measured when the gap between different waveguides is changed equally. Here, the gap between the bus waveguide and ring resonator is changed by keeping the gap between the two ring resonators and gap of the slot region in waveguide constant as illustrated in Fig. 14. Then, altering the gap between the two ring resonatorswhile unchanging the other two gaps as shown in Fig. 15. Finally, Fig. 16 demonstrates the effect of altering slot gap only. The output normalized transmission is found by changing all gaps from 10 *nm* to 300 *nm* with step 5 nm using refractive index of the normal cell for all types of waveguides.

Table 7 Number of supemodes and corresponding sensitivity in the case of slot and hybrid waveguidea when changing both the width of the slot waveguides and the unslotted waveguides

Slot				Hybrid			
w (µm)	ws (µm)	M (modes)	S (nm)	w (µm)	ws (µm)	M (modes)	S (nm)
0.4	0.2	24	63.92	0.4	0.2	24	44.23
0.33	0.16	21	94.72	0.33	0.16	21	55.68
0.26	0.13	19	122.93	0.26	0.13	18	71.34

Table 8 Position of projection in *x* direction and number of supermodes

x	M	x	M
−5.5	6	5.5	6
−5	6	5	6
−4.5	6	4.5	6
−4	6	4	6
−3.5	6	3.5	6
−3	32	3	32
−2.5	22	2.5	22
−2	22	2	22
−1.5	22	1.5	22
−1	17	1	17
−0.5	12	0.5	12
0	12		

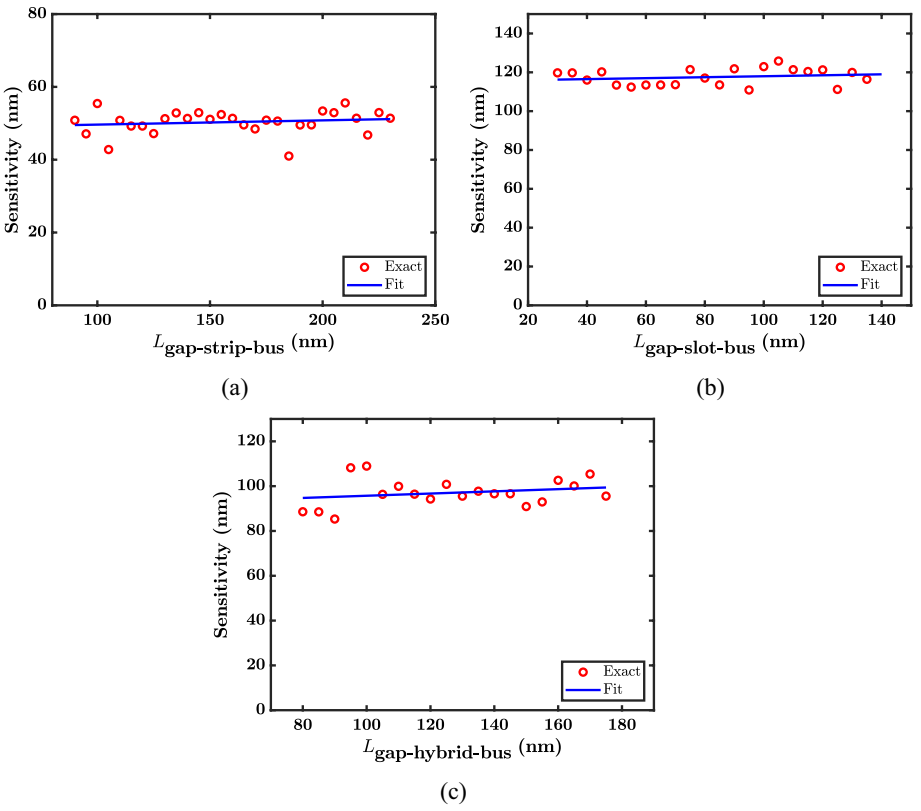

Fig. 14 Sensitivity when changing the bus gap only using: **a** Strip waveguide. **b** Slot waveguide. **c** Proposed hybrid waveguide

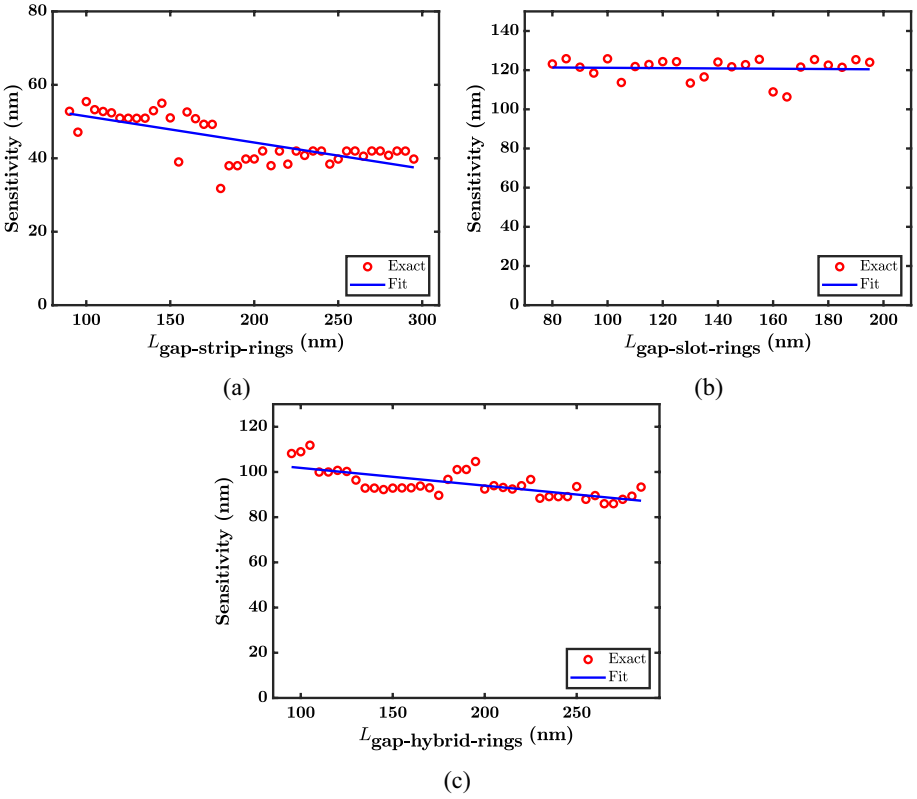

Fig. 15 Sensitivity when changing the rings gap only using: **a** Strip waveguide. **b** Slot waveguide. **c** Proposed hybrid waveguide

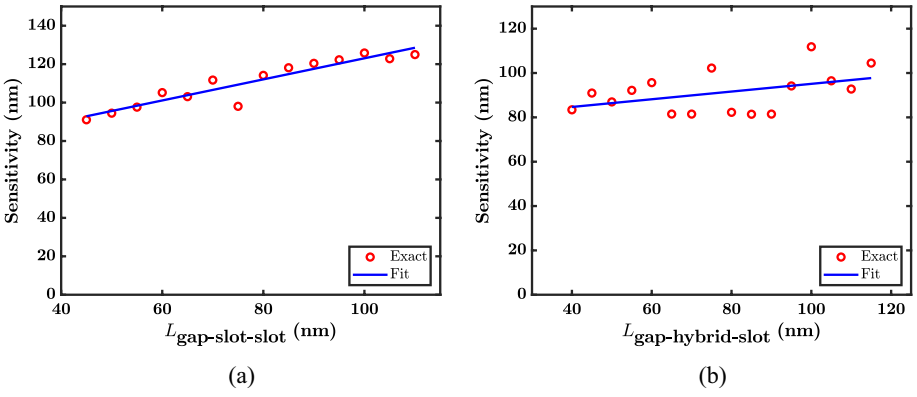

Fig. 16 The sensitivity when changing the slot gap only using **a** Strip-waveguide. **b** Slot-waveguide. **c** Proposed Hybrid-waveguide

4.8 Impact of radius of two ring resonators

In Sect. 4.1, the radius of both ring resonators were altered equally. In this section, the sensitivity is found due to changing each ring resonators radius individually. The output normalized transmission is found by changing the RR radius from 0.4 µm to 6 µm with step 0.1µm for normal cell. Then, the sensitivity is determined in a range such that the output spectrum is readable. Figures 17 and 18 show that no influence on the sensor sensitivity due to altering each radius individually.

5 Conclusion

In this paper, an optical cancer biosensor is proposed using a double ring resonator made of silicon on insulator. The new design is made by using the optimum values of each parameter in the biosensor to get the maximum sensitivity. The performance of the introduced design is proved to be better than previous conventional optical biosensors as it gains the advantages of both strip and slot waveguides. In addition, it has the same size and cost of traditional sensors. Output performance measures, e.g.,

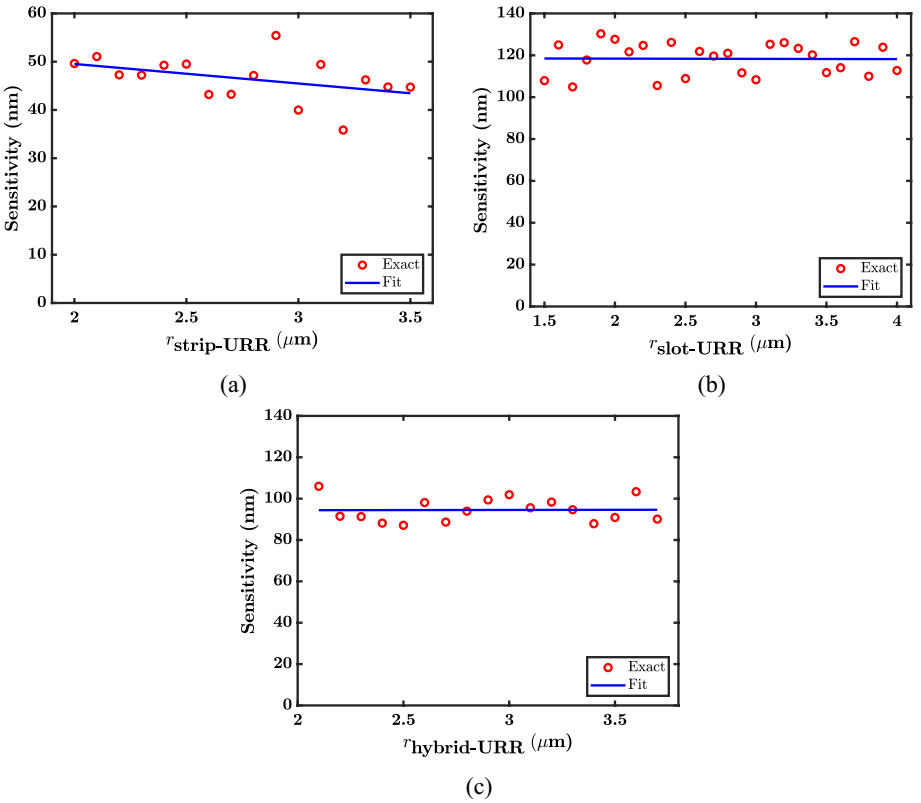

Fig. 17 The sensitivity when changing the radius of upper ring resonator only using **a** Strip-waveguide. **b** Slot-waveguide. **c** Proposed hybrid-waveguide

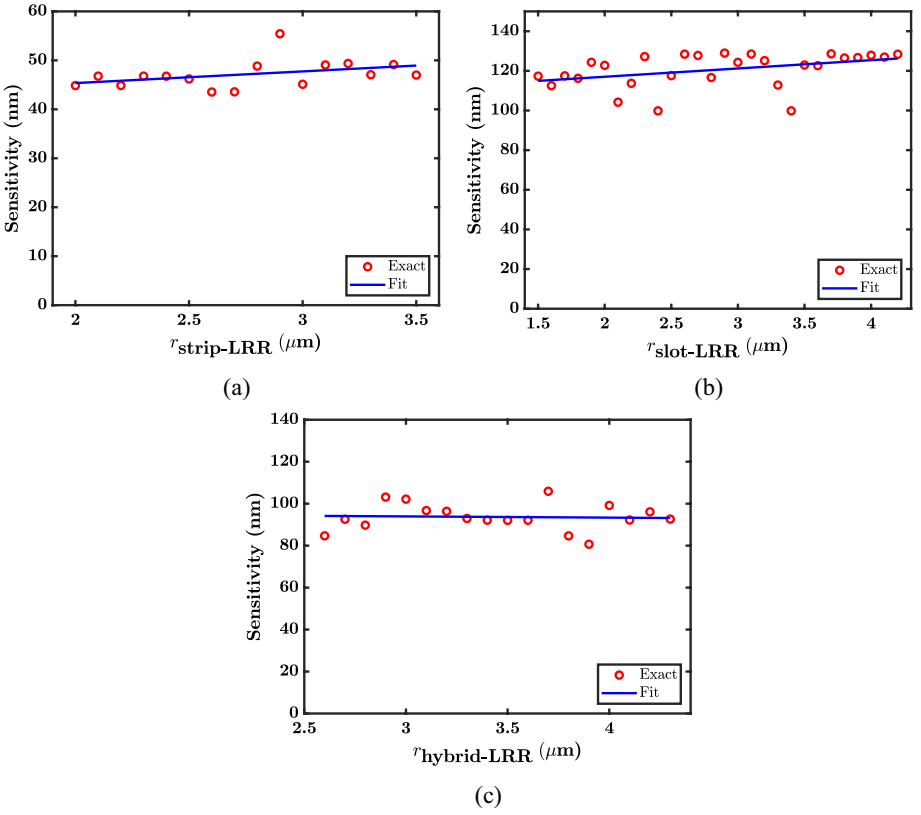

Fig. 18 The sensitivity when changing the radius of lower ring resonator only using **a** Strip-waveguide. **b** Slot-waveguide. **c** Proposed hybrid-waveguide

sensitivity, quality factor, and intrinsic limit of detection, are determined in order to compare between the new design and previous ones. The new design achieves values of 109.8 nm, 537.7, and 0.0255 for sensitivity, quality factor, and limit of intrinsic, respectively. In turned out that this design increases the sensitivity by almost double that of traditional one and it achieves the minimum intrinsic limit of detection than that of both strip and slot waveguides. Our future work will be the fabrication of this proposed biosensor. In addition, study the ratio between the presence of the slot type to the strip type in order to get a higher sensitivity.

Author Contributions Sherine Shawky did the technical work, prepared the figures, and wrote the manuscript. Ahmed H. Abd El-Malek participated in writing the manuscript and reviewing the manuscript. Ahmed Allam participated in reviewing the manuscript. Hossam M. H. Shalaby guided the technical work, participated in writing the manuscript and reviewing it.

Funding Open access funding provided by The Science, Technology & Innovation Funding Authority (STDF) in cooperation with The Egyptian Knowledge Bank (EKB). The license of softwares Lumerical MODE, Lumerical FDTD, and Matlab are supported by our university "Egypt-Japan University of Science and Technology (EJUST)"

Availability of data Not applicable

Declarations

Conflict of interest We have no conflict of interest to declare.

Competing interests The authors declare that they have no competing interests.

References

Ali, L., Mohammed, M.U., Khan, M., Yousuf, A.H., Chowdhury, M.: High-quality optical ring resonator-based biosensor for cancer detection. IEEE Sens. J. **20**(4), 1867–1875 (2020). https://doi.org/10.1109/JSEN.2019.2950664

Azab, M.Y., Hameed, M.F.O., Obayya, S.S.A.: Overview of optical biosensors for early cancer detection: fundamentals, applications and future perspectives. Biology **12**(2), 2079–7737 (2023). https://doi.org/10.3390/biology12020232

Chen, X., Xu, P., Lin, W., Jiang, J., Qu, H., Hu, X.: Cui, Y,: Label-free detection of breast cancer cells using a functionalized tilted fiber grating. Biomed. Opt. Express **13**, 2117–2129 (2022)

De Vos, Katrien, Bartolozzi, Irene, Schacht, Etienne, Bienstman, Peter, Baets, Roel: Silicon-on-insulator microring resonator for sensitive and label-free biosensing. Opt. Express **15**(12), 7610–7615 (2007)

Elsayed, M., Mohamed, S., Aljaber, A., Swillam, M.: Integrated lab-on-a-chip optical biosensor using ultrathin silicon waveguide SOI MMI device. Sensors **20**(17), 4955 (2020). https://doi.org/10.3390/s20174955

Eskandarinezhad, S., Wani, I., Nourollahileilan, M., Khosla, A.: Ahmad, T,: Review-metal and metal oxide nanoparticles/nanocomposites as electrochemical biosensors for cancer detection. J. Electrochem. Soc. **169**, 047504 (2022). https://doi.org/10.1149/1945-7111/ac6076

Ferlay, J., Colombet, M., Soerjomataram, I., Parkin, D., Piñeros, M., Znaor, A., Bray, F.: Cancer statistics for the year 2020: an overview. Int. J. Cancer **149**(4), 778–789 (2021). https://doi.org/10.1002/ijc.33588

Ghasemi, F., Hosseini, E., Song, X., Gottfried, D., Chamanzar, M., Raeiszadeh, M., Adibi, A.: Multiplexed detection of lectins using integrated glycan-coated microring resonators. Biosens. Bioelectron. **80**, 682–690 (2016). https://doi.org/10.1016/j.bios.2016.01.051

Guck, J., Schinkinger, S., Lincoln, B., Wottawah, F., Roenicke, S., Romeyke, M., Bilby, C.: Optical deformability as an inherent cell marker for testing malignant transformation and metastatic competence. Biophys. J. **88**(5), 3689–3698 (2005). https://doi.org/10.1529/biophysj.104.045476

Guo, L., Jackman, J., Yang, H.H., Chen, P., Cho, N., Kim, J.: Strategies for enhancing the sensitivity of plasmonic nanosensors. Nano Today **10**(2), 213–239 (2015). https://doi.org/10.1016/j.nantod.2015.02.007

Guo, Y., Li, H., Reddy, K., Shelar, H., Nittoor, V., Fan, X.: Optofluidic fabry-prot cavity biosensor with integrated flow-through micro-/nanochannels. Appl. Phys. Lett. **98**, 041104–041104 (2011). https://doi.org/10.1063/1.3548673

Haibin, N., Zhang, L., Pin, A., Krasavin, A., Ali, H., Ni, B., Chang, J.: Dual-mode independent detection of pressure and refractive index by miniature grating-coupled surface plasmon sensor. Opt. Express **30**(4), 5758 (2022). https://doi.org/10.1364/OE.446766

Hsieh, M., Thompson, T., Wu, X., Styles, T., O'Flarity, M., Morris, C., Chen, V.: The effect of comorbidity on the use of adjuvant chemotherapy and type of regimen for curatively resected stage III colon cancer patients. Cancer Med. **5**(5), 871–80 (2016). https://doi.org/10.1002/cam4.632

Huang, L., Yan, H., Xu, X., Chakravarty, S., Tang, N., Tian, H., Chen, R.: Improving the detection limit for on-chip photonic sensors based on subwavelength grating racetrack resonators. Opt. Express **25**(9), 10527–10535 (2017). https://doi.org/10.1364/OE.25.010527

Hussain, S., Sánchez, C., Mitchell, A., Deman, A., Laurenceau, E.: Biosensors for circulating tumor cells (ctcs)-biomarker detection in lung and prostate cancer: trends and prospects. Biosens. Bioelectron. **197**, 113770 (2021). https://doi.org/10.1016/j.bios.2021.113770

Kedia, J., Gupta, N.: An FDTD analysis of serially coupled doublering resonator for DWDM. Optik **126**(24), 5641–5644 (2015). https://doi.org/10.1016/j.ijleo.2015.09.031

Kedia, J., Gupta, N.: Numerical simulation of low loss silicon photonic wire waveguide with multiple cladding layers. Opt. Quantum Electron. **49**, 1–14 (2017). https://doi.org/10.1007/s11082-017-1021-8

Kianisarkaleh, A., Lahijani, B., Saberkari, H., Esmaeeli, A.: Optical ring resonators: a platform for biological sensing applications. J. Med. Sig. Sens. **7**(3), 185–191 (2017). https://doi.org/10.4103/jmss.JMSS_9_17

Kumar, V., Kukkar, D., Hashemi, B., Kim, K.H., Deep, A.: Advanced functional structure-based sensing and imaging strategies for cancer detection: possibilities, opportunities, challenges, and prospects. Adv. Funct. Mater. **29**(16), 1807859 (2019). https://doi.org/10.1002/adfm.201807859

Lechuga, L.M.: Biosensors and modern biospecific analytical techniques. Opt. Biosens. **44**, 209–250 (2005)

Long, S., Wang, E., Wu, M., Zhu, H., Nianxi, X., Wang, Y., Cao, J.: Sensing absorptive fluids with backside illuminated grating coupled SPR sensor fabricated by nanoimprint technology. Sens. Actuators A: Phys. **337**, 113416 (2022). https://doi.org/10.1016/j.sna.2022.113416

Mohamed, S., Elsayed, M., Shahada, L., Swillam, M.: Vertical silicon nanowire-based racetrack resonator optical sensor. Appl. Phys. A **125**, 769 (2019). https://doi.org/10.1007/s00339-019-2942-9

Naresh, V., Lee, N.: A review on biosensors and recent development of nanostructured materials-enabled biosensors. Sensors **21**(4), 1109 (2021). https://doi.org/10.3390/s21041109

Nordin, A.: Optical-resonator-based biosensing systems: current status and future prospects. Nanobiosens. Dis. Diagn. **5**, 41–50 (2016). https://doi.org/10.2147/NDD.S70385

Panda, A., Pukhrambam, P.: Photonic crystal biosensor for refractive index based cancerous cell detection. Opt. Fiber Technol. **54**, 102123 (2020). https://doi.org/10.1016/j.yofte.2019.102123

Park, S., Koch, D., Cardenas, R., Käs, J., Shih, C.: Cell motility and local viscoelasticity of fibroblasts. Biophys. J. **89**(6), 4330–4342 (2005). https://doi.org/10.1529/biophysj.104.053462

Ragavendran, L.T., Panchanathan, A., Nayak, C.: Numerical study of temperature and pressure effect on one-dimensional random photonic crystal used as biosensors in the detection of breast cancer cells. Phys. Scripta, **98**(2), 025503 (2023). https://doi.org/10.1088/1402-4896/acad43

Sharifian Jazi, F., Rad, A., Bakhtiari, A., Niazvand, F., Esmaeilkhanian, A., Bazli, L., Moghanian, A.: Biosensors and nanotechnology for cancer diagnosis (lung and bronchus, breast, prostate, and colon): a systematic review. Biomed. Mater. **17**(1), 012002 (2022). https://doi.org/10.1088/1748-605X/ac41fd

Silva, P.P., Meira, D.I., Barbosa, A.C., Costa, D., Rodrigues, M.S., Borges, J., Vaz, F.: Immobilization of streptavidin on a plasmonic au-tio2 thin film towards an LSPR biosensing platform. Nanomaterials, **12**(9), 1526 (2022). https://doi.org/10.3390/nano12091526

Steglich, P., Villringer, C., Pulwer, S., Heinrich, F., Bauer, J., Dietzel, B., Schrader, S.: Hybrid-waveguide ring resonator for biochemical sensing. IEEE Sens. J. **17**, 4781–4790 (2017). https://doi.org/10.1109/JSEN.2017.2710318

Sung, H., Ferlay, J., Siegel, R., Laversanne, M., Soerjomataram, I., Jemal, A., Bray, F.: Global cancer statistics 2020: Globocan estimates of incidence and mortality worldwide for 36 cancers in 185 countries. CA Cancer J. Clin. **71**(3), 209–249 (2021). https://doi.org/10.3322/caac.21660

Suresh, S.: Biomechanics and biophysics of cancer cells. Acta Biomater. **3**(4), 413–438 (2007). https://doi.org/10.1016/j.actbio.2007.04.002

Tan, C., Wang, S., Li, S., Liu, X., Wei, J., Zhang, G., Ye, H.: Cancer diagnosis using terahertz-graphene-metasurface-based biosensor with dual-resonance response. Nanomaterials **12**(21), 3889 (2023). https://doi.org/10.3390/nano12213889

Uddin, M.A., Maswood, M.M.S., Dey, U.K., Alharbi, A.G., Akter, M.: A novel optical micro ring resonator biosensor design using lithium niobate on insulator (lnoi) to detect the concentration of glucose. In 2020 2nd Novel Intelligent and Leading Emerging Sciences Conference (NILES) Giza, 350-354 2020. IEEE.

Vaidyanathan, R., Soon, R., Zhang, P., Jiang, K., Lim, C.: Cancer diagnosis: from tumor to liquid biopsy and beyond. Lab Chip **19**, 11–34 (2018). https://doi.org/10.1039/C8LC00684A

Yan, H., Huang, L., Xu, X., Chakravarty, S., Tang, N., Tian, H., Chen, R.T.: Unique surface sensing property and enhanced sensitivity in microring resonator biosensors based on subwavelength grating waveguides. Opt. Express **24**(26), 29724–29733 (2016). https://doi.org/10.1364/OE.24.029724

Zhao, C.Y., Zhang, L., Zhang, C.: Compact soi optimized slot microring coupled phase-shifted bragg grating resonator for sensing. Opt. Comm. **414**, 212–216 (2018). https://doi.org/10.1016/j.optcom.2018.01.010

Authors and Affiliations

Sherine Shawky[1] · Ahmed H. Abd El-Malek[1] · Ahmed Allam[1] · Hossam M. H. Shalaby[2]

✉ Sherine Shawky
Sherine.Shawky@ejust.edu.eg

Ahmed H. Abd El-Malek
ahmed.abdelmalek@ejust.edu.eg

Ahmed Allam
ahmed.allam@ejust.edu.eg

Hossam M. H. Shalaby
shalaby@ieee.org

[1] Department of Electronics and Communications Engineering, Egypt-Japan University of Science and Technology (E-JUST), Alexandria 21934, Egypt

[2] Electrical Engineering Department, Faculty of Engineering, Alexandria University, Alexandria 21544, Egypt